

The three-dimensional light field within sea ice ridges

Christian Katlein^{1,1}, Jean-Philippe Langelier^{2,2}, Alexandre Ouellet^{2,3}, Félix Lévesque-Desrosiers^{2,3}, Quentin Hisette^{4,4}, Benjamin Allen Lange^{5,5}, Simon Lambert-Girard^{6,6}, Marcel Babin^{7,7}, and Simon Thibault^{2,2}

¹Alfred-Wegener-Institut Helmholtz-Zentrum für Polar- und Meeresforschung

²Centre d'Optique, Photonique et Laser (COPL) and Département de Physique, de Génie Physique et d'Optique, Université Laval

³Centre d'Optique

⁴Hamburg Ship Model Basin (HSVA)

⁵Norwegian Polar Institute

⁶Takuvik Joint International Laboratory, Université Laval and CNRS

⁷Universite laval

November 30, 2022

Abstract

Sea ice pressure ridges have been recognized as important locations for both physical and biological processes. Thus, understanding the associated light-field is crucial, but their complex structure and internal geometry render them hard to study by field methods. To calculate the in- and under-ridge light field, we combined output from an ice mechanical model with a Monte-Carlo ray tracing simulation. This results in realistic light fields showing that light levels within the ridge itself are significantly higher than under the surrounding level ice. Light guided through ridge cavities and scattering in between ridge blocks also results in a more isotropic ridge-internal light field. While the true variability of light transmittance through a ridge can only be represented in ray tracing models, we show that simple parameterizations based on ice thickness and macro-porosity allow accurate estimation of mean light levels available for photosynthesis underneath ridges in field studies and large-scale models.

The three-dimensional light field within sea ice ridges

Christian Katlein^{1,2}, Jean-Philippe Langelier^{2,3}, Alexandre Ouellet³, Félix Lévesque-Desrosiers^{2,3}, Quentin Hissette⁴, Benjamin A. Lange⁵, Simon Lambert-Girard², Marcel Babin², Simon Thibault³

¹Alfred-Wegener-Institut Helmholtz Zentrum für Polar- und Meeresforschung, Bremerhaven, Germany.

²Takuvik Joint International Laboratory, Université Laval and CNRS, Québec, Canada.

³Centre d'Optique, Photonique et Laser (COPL) and Département de Physique, de Génie Physique et d'Optique, Université Laval, Québec, Canada

⁴Hamburg Ship Model Basin (HSVA), Hamburg, Germany.

⁵Norwegian Polar Institute, Fram Centre. Tromsø, Norway

*Corresponding author: Christian Katlein (Christian.Katlein@awi.de)

Key Points:

- Computation of the full three-dimensional light field inside and underneath a pressure ridge
- Enhancement of scalar irradiance within the ridge compared to under level ice
- Simple parameterizations can capture key aspects of the ridge light field e.g. for habitat characterization and large scale models

Abstract (150 words)

Sea ice pressure ridges have been recognized as important locations for both physical and biological processes. Thus, understanding the associated light-field is crucial, but their complex structure and internal geometry render them hard to study by field methods. To calculate the in- and under-ridge light field, we combined output from an ice mechanical model with a Monte-Carlo ray tracing simulation. This results in realistic light fields showing that light levels within the ridge itself are significantly higher than under the surrounding level ice. Light guided through ridge cavities and scattering in between ridge blocks also results in a more isotropic ridge-internal light field. While the true variability of light transmittance through a ridge can only be

31 represented in ray tracing models, we show that simple parameterizations based on ice thickness
32 and macro-porosity allow accurate estimation of mean light levels available for photosynthesis
33 underneath ridges in field studies and large-scale models.

34

35 **Plain Language Summary**

36 When two slabs of sea ice collide, they can break and form pressure ridges by piling up
37 loose ice blocks over each other. The light environment within these ridges is very complicated,
38 but also crucial for their characteristics as habitat for the sea ice ecosystem. We calculate the
39 light field within and underneath such a pressure ridge by tracing the path of many individual
40 photons through the ridge geometry. Our results show, that light levels within the ridge can be
41 higher than in the adjacent undeformed ice. We suggest simple equations that can be used in
42 large scale models to estimate the light intensity underneath the pressure ridge, based on ice
43 geometry data that can be obtained in the field.

44

45 **1. Introduction**

46 Investigating the optical properties of sea ice is an important key to accurately understand
47 the energy transfer across the atmosphere-ice-ocean boundary. Recent changes in the physical
48 properties of the Antarctic and, more notably the Arctic sea ice cover, have resulted in increased
49 light transmittance of the ice pack with important consequences for the physical and biological
50 systems [Meier *et al.*, 2014; Nicolaus *et al.*, 2012]. A large number of studies have investigated
51 the optical properties of sea ice, but most studies focused on undeformed, level and relatively
52 more homogeneous sea ice. While some studies include deformation features such as pressure
53 ridges [Katlein *et al.*, 2019; Lange *et al.*, 2017a; Massicotte *et al.*, 2019], there has been no
54 dedicated investigation of the light field within and underneath these features, besides their
55 general effect of significantly lowering light transmittance.

56 Sea ice pressure ridges form during periods of ice convergence, when two slabs of sea ice
57 collide, shear and break up into blocks that pile up above and below the water line [Davis and
58 Wadhams, 1995; Timco and Burden, 1997]. The portion above the water line is called the ridge
59 sail and is important for snow accumulation and atmospheric turbulence. The 4-5 times thicker
60 portion underneath the water line is called the ridge keel [Timco and Burden, 1997], which

61 determines the hydrodynamic interaction between ice and ocean [Castellani *et al.*, 2015;
62 Castellani *et al.*, 2014], and provides shelter to ice associated flora and fauna [Gradinger *et al.*,
63 2010; Hop *et al.*, 2000; Horner *et al.*, 1992]. Newly formed young ridges are a loose pile of
64 individual ice blocks, characterized by significant macro-pore spaces in between the blocks
65 [Strub-Klein and Sudom, 2012]. This complex geometry of blocks and cavities in a young ridge
66 is very difficult to investigate, but it is exactly this complexity that gives rise to the unique and
67 characteristic physical and biological processes associated with sea ice ridges. With time,
68 thermodynamic processes cause the ridge to refreeze and consolidate in its inner part, while the
69 edges of blocks melt into rounded shapes [Høyland, 2002]. Thus, older ridges transform into
70 more homogeneous, weathered and thick ice bodies – also known as hummocks – over several
71 years [Wadhams and Toberg, 2012].

72 According to diving observations, the complex internal geometry of pressure ridges
73 provides shelter for all trophic levels of the ice associated ecosystem forming a biological
74 hotspot [Assmy *et al.*, 2013; Hop *et al.*, 2000; Horner *et al.*, 1992; Melnikov, 1997; Melnikov and
75 Bondarchuk, 1987; Siegel *et al.*, 1990]. In addition to the ridges housing a particular microbial
76 community [Ackley, 1986], small cavities provide physical protection from larger predators and
77 ocean currents. Various algal communities thrive either hanging between ridge blocks [Lange *et al.*,
78 2017a; Melnikov, 1997] or growing on the upward facing block sides [Fernández-Méndez *et al.*,
79 2018]. On the leeward side of ridges, surface ice relative currents are much reduced
80 increasing the ability of phytoplankton and zooplankton to avoid being flushed away [Katlein *et al.*,
81 2014]. Smaller cavities provide shelter for fish such as the polar cod, while the bigger macro-
82 pores also provide a home and hunting ground for seals [Furgal *et al.*, 1996; Smith *et al.*, 1991].
83 Even polar bears are seeking shelter from the wind in between ridges and hunt for prey in ridge-
84 associated seal lairs [Pilfold *et al.*, 2014]. Overall, pressure ridges are the most prominent and
85 ubiquitous structuring element of the sea ice landscape which despite their very dynamic
86 evolution are home to a condensed and highly productive form of the sea ice associated
87 ecosystem. Due to their high complexity and generally lower light levels, they are however not
88 explicitly included in most large-scale sea ice ecosystem models [Castellani *et al.*, 2017],
89 ignoring their ecological importance.

90 While sea ice thickness in the Arctic is declining [Haas *et al.*, 2008; Kwok and Rothrock,
91 2009] and the ice pack has gotten more dynamic [Rampal *et al.*, 2009], it is uncertain whether

92 the role of sea ice ridges will become more or less important within the Arctic ecosystem. While
93 the proportion of multiyear ice and thus of old ridges is likely to reduce [Maslanik *et al.*, 2007;
94 Maslanik *et al.*, 2011], younger –and thus more porous– ridges are likely to make up the Arctic
95 ice pack in the future [Wadhams and Toberg, 2012]. Investigations of physical properties, such
96 as temperature, salinity and strength of pressure ridges, have been conducted intensively, as the
97 mechanical properties are of commercial interest to shipping and offshore operations
98 [Leppäranta and Hakala, 1992; Richter-Menge and Cox, 1985; Strub-Klein and Sudom, 2012].
99 Underwater investigations of ridges have only recently been aided by robotic vehicles
100 [Fernández-Méndez *et al.*, 2018; Katlein *et al.*, 2014; Lange *et al.*, 2017a].

101 Light is one of the main drivers particularly of the autotrophic portion of the ice
102 associated ecosystem, and it is very important to understand the nature and amount of light
103 present within the ecological hotspots of ridge cavities. However, radiative transfer in such
104 complex geometries cannot be investigated with the typical one-dimensional radiative transfer
105 models, as they are only formulated for homogeneous slabs of ice [Katlein *et al.*, 2016]. Only
106 few studies explicitly investigate the general decrease in light transmission due to the larger
107 thickness of ridges [Lange *et al.*, 2019; Lange *et al.*, 2017b] or try to parameterize it for model
108 calculations [Fernández-Méndez *et al.*, 2018; Lange *et al.*, 2017a]. To improve habitat
109 characterization and the representation of pressure ridges in ecological models, it is necessary to
110 improve our understanding of radiative transfer in complex ridge geometries.

111 The objective of our work is to explicitly model the light field geometry within and
112 underneath a typical young pressure ridge. As field data of the full internal geometry of a
113 pressure ridge are not yet available, we use an artificial ridge generated in an ice mechanical
114 model as input for a three-dimensional ray-tracing radiative transfer model. As this is not a
115 representation of a real-world scenario, our main focus lies on understanding the radiative
116 transfer processes governing the light field inside the ridge, and not the absolute value of light
117 transmittance. Analysis of model output also allows for the comparison of existing and new
118 parameterizations of radiative transfer through sea ice pressure ridges.

119 2. Materials and Methods

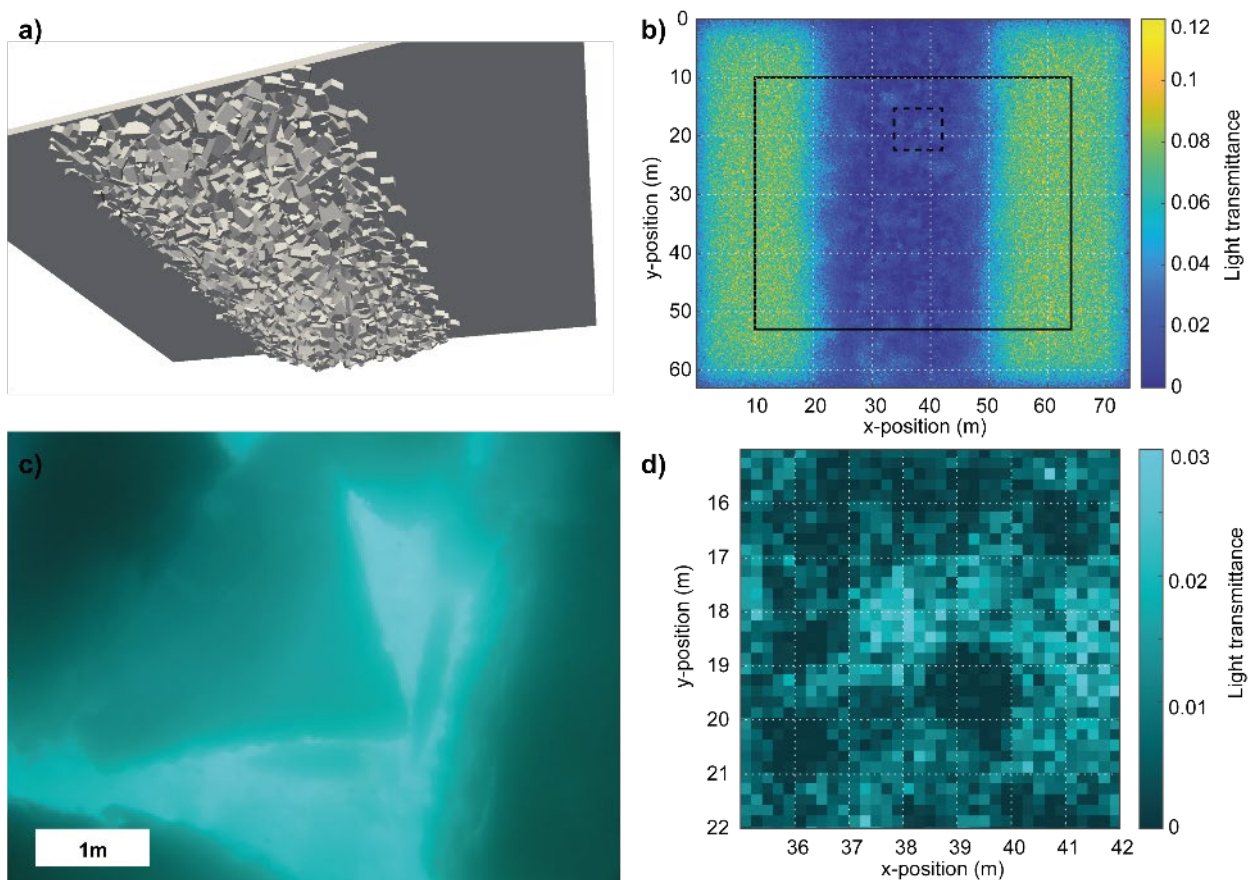
120 2.1 Sea ice model and the investigated ridge

121 There are plenty of available datasets from surface laser scanning and underwater
122 multibeam sonar surveys that can provide the full three-dimensional external geometry of
123 pressure ridges [*Melling et al.*, 1993; *Williams et al.*, 2013; *Williams et al.*, 2015]. However,
124 none of these studies provide insight into the internal structure of these complex ice geometries.
125 Extensive drilling surveys [*Høyland*, 2002; *Strub-Klein and Sudom*, 2012] or geophysical
126 methods, such as electromagnetic induction sounding [*Hunkeler et al.*, 2016] and nuclear
127 magnetic resonance [*Nuber et al.*, 2017; *Rabenstein et al.*, 2013] can provide some information
128 on the internal ridge structure. The spatial resolution and contrast of these data are, however, not
129 sufficient as input data for precise three-dimensional radiative transfer modeling.

130 To overcome this lack of data, we use an artificially created ridge geometry from a
131 mechanical sea ice model used for simulating the interaction of sea ice with ships and structures
132 [*Hisette et al.*, 2017]. In this model, a ridge is created using the “floating-up” technique, where
133 buoyant ice blocks are released underneath a level ice sheet of 1m thickness and afterwards
134 formed into a ridge of triangular cross section. During the forming process, the ice blocks are
135 pressed against each other so that a realistic ice-water porosity level is reached (An animation of
136 this process can be found here: <https://www.youtube.com/watch?v=Zwn2J39EOIA>). This
137 creation mechanism results in a ridge without sail (Figure 1a), but the continuous ice sheet comes
138 closer to a partly consolidated ridge than a simulation where ridge blocks are piled up by moving
139 two ice sheets against each other. The ridge construction method has proved to produce realistic
140 ridge geometries for ship-ice interaction modeling and ice tank testing [*Hisette et al.*, 2017] and
141 its geometric properties compare well to existing literature: The achieved macro-porosity of 35%
142 and a ridge keel depth to keel width ratio around 4 is in line with ridge observations and the
143 block length is in the correct relation to the sheet ice thickness [*Strub-Klein and Sudom*, 2012;
144 *Timco and Burden*, 1997]. Also the ratio of keel depth and block thickness fit previous
145 observations and mechanical modeling [*Parmarter and Coon*, 1972]. Of course, this ridge can
146 only approximate a realistic situation, as many real processes, such as consolidation and snow
147 accumulation are not taken into account. The geometric size of the model domain (Figure 1b) is
148 74m by 63m with a maximum ridge keel depth of 6.64 m.

149

150



151

152 **Figure 1.** a) rendering of the investigated three-dimensional ridge geometry b) downward planar
 153 irradiance field at 4m depth as computed by the ray-tracing model. The black rectangle depicts
 154 the area used for data analysis. c) Upward looking photo taken by a remotely operated vehicle on
 155 19 August 2018 during the AO18 expedition with the Swedish icebreaker Oden from
 156 approximately 10m depth. d) Close-up of the modeled irradiance field (dashed box in b)) at a
 157 comparable spatial scale to the photograph in c) with color bar adjusted to the picture colors.
 158 Individual ridge blocks are clearly discernible.

159

2.2 Optical Model

160

161 The three-dimensional ridge geometry from the mechanical ice model was directly used
 162 in the optical design software Zemax Optic-Studio (Zemax LLC, Kirkland, USA). Ray tracing
 163 was performed with a total number of $5 \cdot 10^7$ rays using a diffuse lambertian light source
 164 representative of typical cloudy conditions in the summer sea ice area. We assigned homogenous
 165 optical properties to the ice resulting in broadband transmittance of 0.074 and albedo of 0.72 for

166 the 1m thick level ice sheet which is comparable to published literature values [Katlein *et al.*,
 167 2019; Katlein *et al.*, 2021; Light *et al.*, 2008; Light *et al.*, 2015] . The Lambertian light source
 168 emitted a realistic solar spectrum, and a database of measured real and imaginary refractive
 169 indices for ice was used [Warren and Brandt, 2008]. The water was assumed to be free of
 170 scatterers, representing typical clear Arctic waters [Katlein *et al.*, 2016; Pavlov *et al.*, 2017;
 171 Taskjelle *et al.*, 2017]. The scattering coefficient of the ice was set to $\kappa_{si} = 200 \text{ m}^{-1}$ and we
 172 adopted a Henyey-Greenstein phase function with asymmetry parameter $g = 0.94$. For the real
 173 and imaginary refractive index of water we used the database “Water” built into Optic-Studio
 174 stock materials catalog MISC. Total scalar (E_0) and downwelling planar irradiances (E_d) were
 175 calculated at a spatial resolution of 0.2 by 0.2 m by the model at horizontal levels of 0, 1, 2, 3, 4,
 176 5 and 6 m depth, both within the ice and in the underlying water. Downwelling planar irradiance
 177 E_d quantifies the energy flux across a horizontal area, and thus includes a cosine weighting of
 178 rays depending on zenith angle. Total scalar irradiance E_0 quantifies the energy flux through a
 179 point integrating equally weighted rays from all directions. We define the ratio $m = E_d/E_0$,
 180 which is similar to the mean cosine $\mu = E_{net}/E_0$ [Mobley, 1994] and is a rough index describing
 181 the geometric shape of the angular radiance distribution.

182 To overcome edge effects of the discrete ray tracing simulation, only the central part of
 183 the simulated ridge was used in the following evaluation (Figure 1b). The resulting light fields
 184 closely resemble upward looking images obtained from under-ice ROV dives (Figure 1 c, d)
 185 showing that light field calculations of the ray tracing model generate realistic results.

186 **2.3 Light field parameterizations**

187 Most light transmittance parameterizations have been designed for level ice. Sea ice is
 188 often modeled as a plane parallel medium with homogenous material properties within one or
 189 several layers [Mobley *et al.*, 1998; Perovich, 1990]. Only simple parameterizations based on the
 190 exponential decay of light in a medium [Bouguer, 1729; Lambert, 1760] have been applied to the
 191 more complex situation for old ridges [Lange *et al.*, 2017a] and young ridges [Fernández-
 192 Méndez *et al.*, 2018].

193 The first parameterization that we evaluate in this study is the simple bulk-exponential
 194 approach. Light transmittance T is defined as the ratio of downwelling planar irradiance

195 transmitted through the ice E_d divided by incoming downwelling planar irradiance at the ice
 196 surface E_i :

$$197 \quad T = \frac{E_d}{E_i} \quad (1)$$

198 In its most simple form of a uniform slab of ice light transmittance can be parameterized as
 199 [Katlein *et al.*, 2015; Lange *et al.*, 2017a]

$$200 \quad T = (1 - \alpha) \cdot \exp(-\kappa_{d,ice} \cdot z), \quad (2)$$

201 where α is the surface albedo and z the total bulk ice thickness. In our model setup of level ice
 202 without vertically varying optical properties, the optical properties described in section 2.2 yield
 203 a vertical attenuation coefficient for ice of $\kappa_{d,ice} = 1.33 \text{ m}^{-1}$.

204 For the more complex geometry of pressure ridges Fernández-Méndez *et al.* [2018] separated
 205 this formulation into a piecewise exponential plane parallel model, taking into account water
 206 pockets within the ice and several layers of ridge blocks. Adjusting their parameterization to our
 207 more idealized ridge results in

$$208 \quad T = (1 - \alpha) \cdot \exp(-\kappa_{d,ice} \cdot (z_{ice,1} + z_{ice,2} + \dots) - \kappa_{d,w} \cdot (z_{w,1} + z_{w,2} + \dots)). \quad (3)$$

209 Here $z_{ice,1} + z_{ice,2} + \dots = \sum_{i=1}^n z_{ice,i}$ describes the sum of ice thickness associated with n
 210 individual ridge blocks and $z_{w,1} + z_{w,2} + \dots$ the respective geometric thickness of water in the
 211 ridge voids. In the following the first is referred to as the partial ice thickness, which can also be
 212 imagined as the amount of ice that would need to be drilled during a vertical ridge drilling
 213 exercise. While this formulation seems to explicitly account for a more realistic ice geometry, it
 214 clearly neglects laterally traveling light. Total bulk ice thickness z (including voids) and partial
 215 ice thickness were extracted from the simulated ridge geometry (described in section 2.1) in all
 216 locations across the ridge. The average vertical attenuation coefficient in the water $\kappa_{d,w} =$
 217 0.02 m^{-1} was determined from our simulation by fitting an exponential decay to the light field
 218 underneath level ice. The respective light transmittance was then calculated for each point using
 219 the above parameterization to allow for a comparison to the fully three-dimensional ray tracing
 220 model.

221 **3. Results and Discussion**

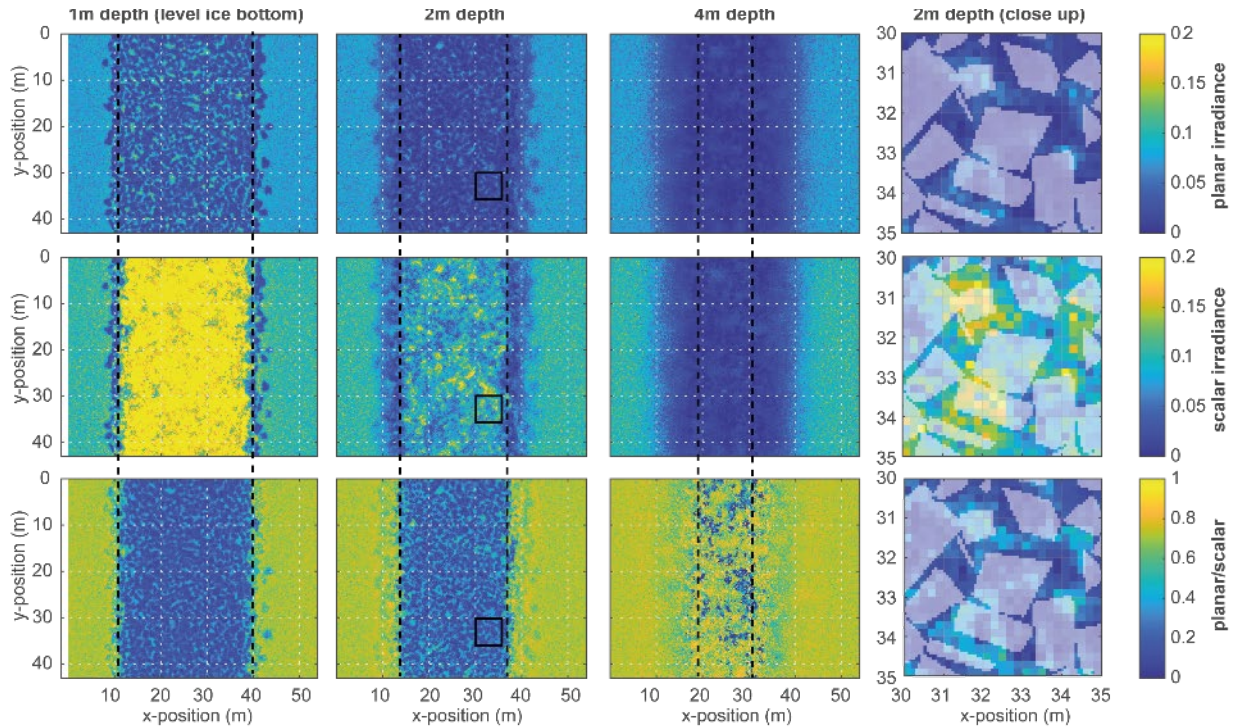
222 **3.1 Calculated light field**

223 The calculated light fields resulting from the ray-tracing calculations are shown in Figure
224 2. Apart from the slow decay of light with depth under level ice due to water absorption, the
225 model also reproduces the general effect of lower light transmittance underneath the pressure
226 ridge. Distinct shadows by individual ridge blocks are visible. These are also evident from
227 upward looking ROV images providing validation to our model results (Figure 1c).

228 A main result from these calculations is that the scalar irradiance within the pressure
229 ridge is considerably higher than at the same depth underneath level ice, particularly in the upper
230 half of the ridge. This effect is caused by two factors. First, water filled cavities in the ridge lead
231 to less total light attenuation. Second, the strong multiple scattering between ridge blocks
232 changes the light field shape towards a more isotropic radiance distribution. This increases
233 particularly the total scalar irradiance versus downwelling planar irradiance (Figure 2), as
234 evident by the decreased mean cosine (section 3.2). Thus, light levels within ridge cavities are
235 similarly high as within ridge blocks. These significantly higher light levels provide pelagic and
236 ice associated algae and zooplankton with favorable light conditions within the ridge cavities. In
237 their interior, ridges thus represent areas of higher light availability compared to the
238 surroundings. In addition, macro pore space increases the habitable volume of the ridge offering
239 also increased areas of ice surfaces as substrate. Only underneath, ridge keels shade the light
240 field and decrease light transmittance. This particular light regime might further enhance positive
241 factors such as the physical protection from currents and predators that the ridge associated
242 ecosystem can benefit from [*Gradinger et al.*, 2010].

243

244



245

246 **Figure 2:** Horizontal slices of the calculated light field, within and underneath the ridge. Top
 247 row: planar downwelling irradiance (normalized to ice surface) at the depths of 1m, 2m, and 4m
 248 as well as a close up of the 2m depth at a representative spot (black rectangles) within the ridge
 249 flank. Second row: Scalar irradiance. Third row: the ratio $m = E_d/E_0$ indicating the geometry
 250 of the light field. The area between the black dashed lines indicates the approximate region,
 251 where the horizontal slice lies within the ridge body.

252

253 3.2 Geometry of the light field in and underneath the ridge

254 Here, we use the ratio $m = E_d/E_0$ as a descriptor of the light field geometry. It
 255 describes the radiance distribution geometry between the two extreme cases of isotropic ($m =$
 256 **0.25**) and unidirectional downwelling ($m = 1$) light fields. Values of $m < 0.25$ resemble a
 257 stronger upwelling portion of the light field caused by the upward-scattering of laterally
 258 travelling photons. Note, that this definition is different to the more common definition of the
 259 mean cosine of the downwelling light field as used in Matthes et al. [2019]. It is however
 260 equivalent in the absence of upwelling light, e.g. here under the level ice portion. As already
 261 mentioned above, multiple scattering within and in between ridge blocks bounces downwelling
 262 light back upwards within the ridge, while the low amount of scattering in the water column
 263 reduces upwelling light underneath ice. Organisms within the ridge thus receive similar amounts

264 of light from all directions enhancing light availability for photosynthesis. Our model produces
265 values of $m = 0.72$ comparable to the mean cosines shown by Matthes et al. [2019] for level ice
266 (Figure 2). It also reproduces the known slow increase of the mean cosine with depth. Within the
267 ridge, however, values are significantly lower. Values around $m = 0.1 - 0.3$ indicate an
268 isotropic or directional in-ridge light field, where a majority of the light travels horizontally and
269 not in downwelling direction. Inside the ridge, values increase from $m = 0.1 - 0.3$ inside the
270 upper part of the ridge over $m = 0.2 - 0.4$ at the bottom of the ridge to $m = 0.7 - 0.8$ for
271 regions below the ridge. Knowledge of these ratios enables derivation of scalar irradiance levels
272 within ridges from the parameterizations of downwelling planar irradiances.

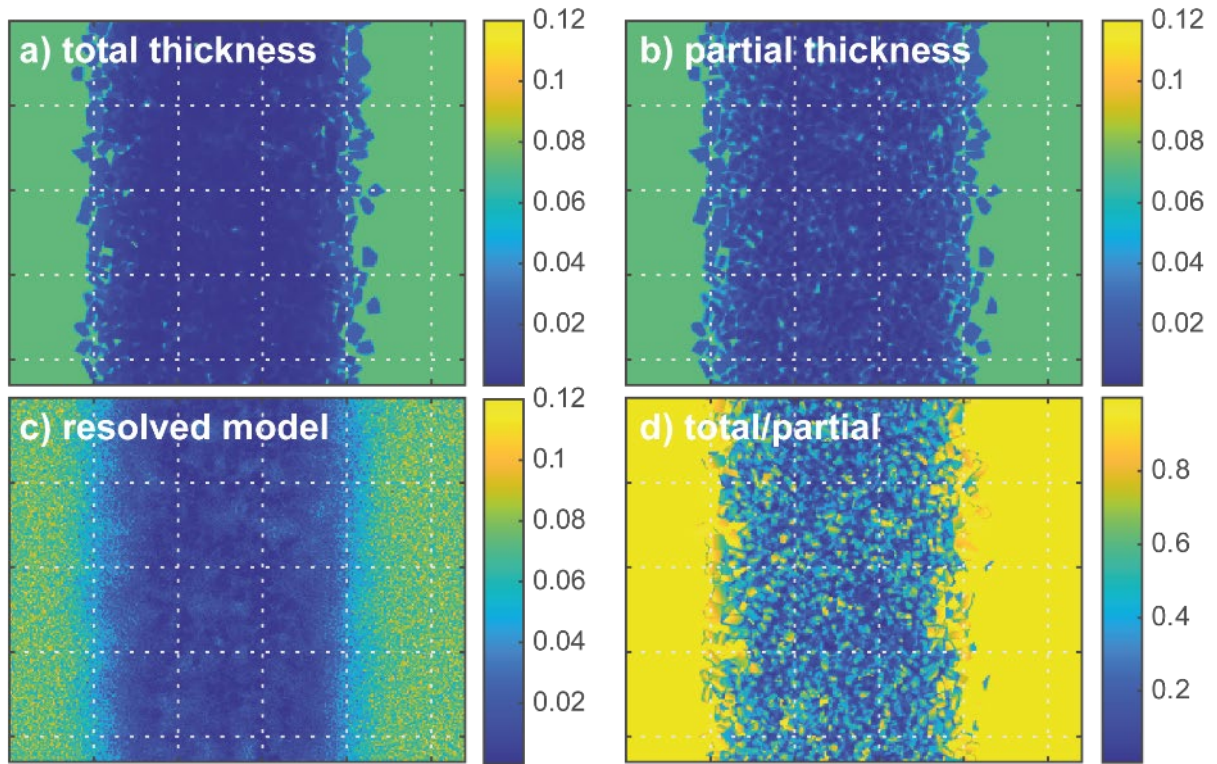
273 **3.3 Comparison to simple ridge models**

274 Figure 3 evaluates the simple parameterizations of light transmission presented in section
275 2.3. Transmittance parameterized on the basis of total ice thickness is expectedly lower than
276 transmittance parameterized on the basis of partial ice thickness (Figure 3). Both
277 parameterizations do not appropriately account for lateral smoothing of light transmittance
278 pointing to the fact that estimations of the light field within a ridge from drill holes can both
279 over- and underestimate the actual light intensity. This is caused by the strong variability of
280 partial and total ice thickness along the ridge given by the chaotic block structure (Figure 4a).

281 Across ridge light profiles show a significant variability linked directly to local ridge
282 block geometries (Figure 4b). Deviations are most prominent when ridge cavities of large
283 vertical extent act as light guides through the ridge. While in our scenario we are able to evaluate
284 local partial and total ice thickness in each spot, this will not be possible in a real setting, where
285 ridge macroporosity data is acquired by ridge drilling. It is, however, evident that mean across-
286 ridge light transmittance between raytracing and exponential models fit reasonably well. The
287 parameterization using total ice thickness underestimates light transmittance, while the
288 parameterization using partial ice thickness comes much closer to the average. Thus,
289 parameterizations based on partial ice thickness will yield more realistic results. Both
290 parameterizations fail to reproduce the light field at the outer ridge slopes, which are
291 significantly smoother in the full three-dimensional simulation, than in the average
292 parameterizations due to horizontal light propagation (Figure 4). For most large-scale models
293 such inaccuracies would be acceptable, while more targeted modeling e.g. supporting in-situ

294 sampling could suffer from undetected light field variability driven by specific local ridge
 295 geometry.

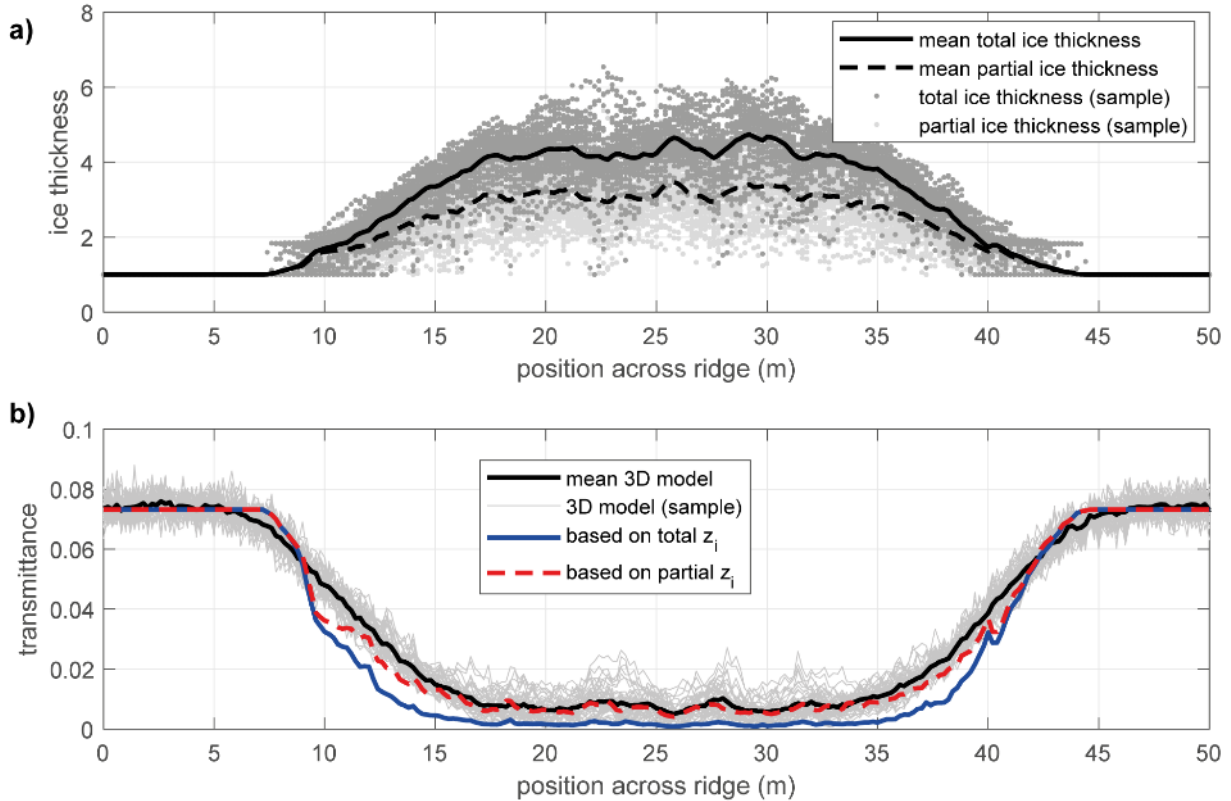
296



297

298 **Figure 3:** Light field at 5m depth as parameterized based on total ice thickness (a), partial ice
 299 thickness (b) and derived from the fully resolved three-dimensional raytracing model (c). Panel
 300 d) shows the ratio of the parameterizations based on total and partial sea ice thickness.

301



302

303 **Figure 4:** a) Across-ridge profiles of mean total (solid line) and partial (dashed line) ice
 304 thickness. Light and dark grey dots represent individual pixels of partial and total ice thickness
 305 respectively. b) Across ridge planar irradiance profiles: mean planar irradiance transmittance
 306 (solid black line) and individual profiles of planar irradiance transmittance at 5m depth from
 307 raytracing (thin grey lines), and parameterized using partial (dashed blue line) and total ice
 308 thicknesses (solid blue line).

309 **3.4 Potential impact of the ridge sail and consolidated layer**

310 In our model setup, the introduction of a simple idealized ridge sail did not show any
 311 significant effect. However, in reality a ridge sail may have additional influences on the light
 312 field within and under the ridge keel by influencing the distribution of snow around the sail,
 313 and/or the additional geometric effects and scattering of light within the surface ice blocks and
 314 air gaps of the sail. Snow distribution is largely controlled by the surface topography of the sea
 315 ice where snow is removed from high points (e.g., ridge sails and hummocks) and accumulates in
 316 low points or adjacent to high points (e.g., around ridge sails) [Lange *et al.*, 2019; Sturm *et al.*,
 317 2002]. This can result in thick snow accumulation around ridges, typically greater than 0.5 m,
 318 substantially reducing the absolute amount of light penetrating into the ridge from the top and
 319 further increasing the importance of both lateral light transfer and light guided through voids.

320 This snow distribution is often asymmetrical due to prevailing wind directions, with more snow
321 accumulating on the lee side of the ridge. The ridge sail, on the other hand, can have substantial
322 regions of thin and snow-free ice protruding from the otherwise snow-covered ridge sail, which
323 may have an opposite influence on the light field by locally increasing light penetration into the
324 ridge. Also, the geometry of the surface blocks (i.e., angle relative to the solar inclination) may
325 further increase light penetration into the ridge by decreasing the effective angle of sun
326 inclination and minimizing specular reflection.

327 While the investigated ridge geometry somewhat mimics a thin consolidated layer, the
328 amount of consolidation inside a ridge will certainly impact the light field. Consolidation will
329 close voids, that before acted as light guides and will further reduce light transmission through
330 the ridge by reducing its macro-porosity. This effect would be included in light estimates derived
331 from light transmission parameterizations accounting for the macro-porosity of a ridge. These
332 potential impacts and uncertainties should be included and assessed in future modeling studies
333 and field measurements in order to quantify their respective effects.

334 **4. Summary**

335 We presented the first full three-dimensional modeling of the light field in a young
336 pressure ridge. Model results are comparable to observations from upward looking under-ice
337 cameras and thus are likely representative of a typical real-world situation. Light levels within
338 ridge cavities are up to three times higher than in the surrounding waters, thus enhancing the
339 ecological importance of pressure ridges for the sea ice system. The ridge light field is
340 characterized by an isotropic or even upwelling radiance distribution with low values of the
341 mean cosine. Particularly these presented ratios of planar and scalar irradiance inside the ridge
342 will be of use when estimating light available for photosynthesis to convert between the different
343 light field quantities. The high spatial variability of ridge block geometry can only be addressed
344 correctly in a full ray tracing calculation, but simple parameterizations provide a reasonable
345 mean estimate of both light transmittance and spatial variability. Parameterizations based on
346 partial ice thickness yield more realistic results by accounting for macro-porosity of the ridge
347 structure. It is also evident that such simple parameterizations cannot correctly reproduce the
348 light field at the edge of ridges due to the importance of lateral light propagation.

349 The presented parameterizations are a simple way to estimate light levels inside a
350 pressure ridge to ease habitat characterization and derive ridge associated photosynthetic
351 production. Due to their simplicity, they can be used based on the results of traditional ridge
352 drilling surveys, but also could be applied to large scale sea-ice ecosystem models.

353 The full internal structure of pressure ridges as used for our study, is hard to acquire from
354 field data. Further and more complex ray-tracing simulations of realistic scenarios of the light
355 field in ridges could be based on the combined use of surface laser scanning, snow mapping and
356 under-ice multibeam sonar mapping. This will require an indirect consideration of ridge internal
357 geometry using measured macro-porosities from drilling data. Further simulations based on
358 different ice mechanical ridge formation models could evaluate numerous scenarios tailored to
359 specific observed ridge characteristics. When coupled with a snow-drift model, this might also
360 allow some insight into the complex interplay of ridge sails and snow accumulation and their
361 effect on the light field under and within the ridge. As fully resolved field data will likely not
362 become available soon, the simple parameterizations considering average ridge macro-porosity
363 derived here will allow for reasonable estimates of the light field around pressure ridges. This
364 will aid both, in-situ habitat characterization, as well as large-scale modeling to provide realistic
365 light fields to ridge.

366 **Acknowledgments**

367 The writing of this manuscript was supported by a postdoctoral research fellowship to CK by
368 Sentinel North supervised by Marcel Babin and Simon Thibault. The ROV work was funded by
369 the Helmholtz Infrastructure Initiative “Frontiers in Arctic Marine Monitoring (FRAM)” and the
370 Alfred-Wegener Institute. ROV observations during the AO18 expedition were supported by
371 captain and crew of icebreaker Oden and the Swedish Polar Research Secretariat (SPRS). BAL is
372 supported by funding from the Research Council of Norway projects: CAATEX [280531] and
373 HAVOC [280292]. We thank Mario Hoppmann, Philipp Anhaus and Matthieu Labaste for their
374 help in conducting the ROV observations. The modeled light fields are available at
375 <https://doi.org/10.5281/zenodo.4491700> [Katlein and Langelier, 2021].

376 **Author contribution statement**

377 CK and SLG developed the concept for this study. QH provided the ridge geometry, JPL, AO
378 and FLD ran the ray tracing simulations with Zemax. BAL, MB, ST provided guidance,

379 interpretation and discussion of data and results. CK wrote and all authors contributed to editing
 380 of the manuscript.

381

382 **References**

383

384 Ackley, S. (1986), Sea-ice pressure ridge microbial, *Antarctic Journal of the United States*,
 385 *21*(5), 172.

386 Assmy, P., et al. (2013), Floating Ice-Algal Aggregates below Melting Arctic Sea Ice, *PLoS*
 387 *ONE*, *8*(10), e76599, doi:10.1371/journal.pone.0076599.

388 Bouguer, P. (1729), *Essai d'Optique*, Claude Jombert.

389 Castellani, G., R. Gerdes, M. Losch, and C. Lüpkes (2015), Impact of Sea-Ice Bottom
 390 Topography on the Ekman Pumping, in *Towards an Interdisciplinary Approach in Earth System*
 391 *Science: Advances of a Helmholtz Graduate Research School*, edited by G. Lohmann, H.
 392 Meggers, V. Unnithan, D. Wolf-Gladrow, J. Notholt and A. Bracher, pp. 139-148, Springer
 393 International Publishing, Cham, doi:10.1007/978-3-319-13865-7_16.

394 Castellani, G., M. Losch, B. A. Lange, and H. Flores (2017), Modeling Arctic sea-ice algae:
 395 Physical drivers of spatial distribution and algae phenology, *Journal of Geophysical Research:*
 396 *Oceans*, *122*(9), 7466-7487, doi:10.1002/2017jc012828.

397 Castellani, G., C. Lüpkes, S. Hendricks, and R. Gerdes (2014), Variability of Arctic sea-ice
 398 topography and its impact on the atmospheric surface drag, *Journal of Geophysical Research:*
 399 *Oceans*, *119*(10), 6743-6762, doi:<https://doi.org/10.1002/2013JC009712>.

400 Davis, N. R., and P. Wadhams (1995), A statistical analysis of Arctic pressure ridge morphology,
 401 *Journal of Geophysical Research: Oceans*, *100*(C6), 10915-10925, doi:10.1029/95jc00007.

402 Fernández-Méndez, M., et al. (2018), Algal Hot Spots in a Changing Arctic Ocean: Sea-Ice
 403 Ridges and the Snow-Ice Interface, *Frontiers in Marine Science*, *5*(75),
 404 doi:10.3389/fmars.2018.00075.

405 Furgal, C. M., K. M. Kovacs, and S. Innes (1996), Characteristics of ringed seal, *Phoca hispida*,
 406 subnivean structures and breeding habitat and their effects on predation, *Canadian Journal of*
 407 *Zoology*, *74*(5), 858-874, doi:10.1139/z96-100.

408 Gradinger, R., B. Bluhm, and K. Iken (2010), Arctic sea-ice ridges-Safe heavens for sea-ice
 409 fauna during periods of extreme ice melt?, *Deep-Sea Research Part Ii-Topical Studies in*
 410 *Oceanography*, *57*(1-2), 86-95, doi:10.1016/j.dsr2.2009.08.008.

411 Haas, C., A. Pfaffling, S. Hendricks, L. Rabenstein, J.-L. Etienne, and I. Rigor (2008), Reduced
 412 ice thickness in Arctic Transpolar Drift favors rapid ice retreat, *Geophys. Res. Lett.*, *35*(17),
 413 L17501, doi:10.1029/2008gl034457.

- 414 Hisette, Q., A. Alekseev, and J. Seidel (2017), Discrete Element Simulation of Ship Breaking
 415 Through Ice Ridges, in *The 27th International Ocean and Polar Engineering Conference*, edited,
 416 p. 9, International Society of Offshore and Polar Engineers, San Francisco, California, USA.
- 417 Hop, H., M. Poltermann, O. J. Lønne, S. Falk-Petersen, R. Korsnes, and W. P. Budgell (2000),
 418 Ice amphipod distribution relative to ice density and under-ice topography in the northern
 419 Barents Sea, *Polar Biol.*, 23(5), 357-367, doi:10.1007/s003000050456.
- 420 Horner, R., S. F. Ackley, G. S. Dieckmann, B. Gulliksen, T. Hoshiai, L. Legendre, I. A.
 421 Melnikov, W. S. Reeburgh, M. Spindler, and C. W. Sullivan (1992), Ecology of Sea Ice Biota .1.
 422 Habitat, Terminology, and Methodology, *Polar Biol.*, 12(3-4), 417-427.
- 423 Høyland, K. V. (2002), Consolidation of first-year sea ice ridges, *Journal of Geophysical*
 424 *Research: Oceans*, 107(C6), 15-11-15-16, doi:10.1029/2000jc000526.
- 425 Hunkeler, P. A., M. Hoppmann, S. Hendricks, T. Kalscheuer, and R. Gerdes (2016), A glimpse
 426 beneath Antarctic sea ice: Platelet layer volume from multifrequency electromagnetic induction
 427 sounding, *Geophys. Res. Lett.*, 43(1), 222-231, doi:10.1002/2015gl065074.
- 428 Katlein, C., S. Arndt, H. J. Belter, G. Castellani, and M. Nicolaus (2019), Seasonal Evolution of
 429 Light Transmission Distributions Through Arctic Sea Ice, *Journal of Geophysical Research:*
 430 *Oceans*, 124, doi:<https://doi.org/10.1029/2018JC014833>.
- 431 Katlein, C., et al. (2015), Influence of ice thickness and surface properties on light transmission
 432 through Arctic sea ice, *Journal of Geophysical Research: Oceans*, 120(9), 5932-5944,
 433 doi:10.1002/2015JC010914.
- 434 Katlein, C., M. Fernández-Méndez, F. Wenzhöfer, and M. Nicolaus (2014), Distribution of algal
 435 aggregates under summer sea ice in the Central Arctic, *Polar Biol.*, 1-13, doi:10.1007/s00300-
 436 014-1634-3.
- 437 Katlein, C., and J.-P. Langelier (2021), Computed Light Fields Within a Sea Ice Pressure Ridge,
 438 edited, Zenodo, doi:10.5281/zenodo.4491701.
- 439 Katlein, C., D. K. Perovich, and M. Nicolaus (2016), Geometric Effects of an Inhomogeneous
 440 Sea Ice Cover on the under Ice Light Field, *Frontiers in Earth Science*,
 441 doi:10.3389/feart.2016.00006.
- 442 Katlein, C., L. Valcic, S. Lambert-Girard, and M. Hoppmann (2021), New insights into radiative
 443 transfer within sea ice derived from autonomous optical propagation measurements, *The*
 444 *Cryosphere*, 15(1), 183-198, doi:10.5194/tc-15-183-2021.
- 445 Kwok, R., and D. A. Rothrock (2009), Decline in Arctic sea ice thickness from submarine and
 446 ICESat records: 1958-2008, *Geophys. Res. Lett.*, 36, doi:10.1029/2009gl039035.
- 447 Lambert, J. H. (1760), *Photometria*.

- 448 Lange, B. A., et al. (2017a), Pan-Arctic sea ice-algal chl a biomass and suitable habitat are
 449 largely underestimated for multiyear ice, *Global Change Biology*, 23(11), 4581-4597,
 450 doi:10.1111/gcb.13742.
- 451 Lange, B. A., et al. (2019), Contrasting Ice Algae and Snow-Dependent Irradiance Relationships
 452 Between First-Year and Multiyear Sea Ice, *Geophys. Res. Lett.*, 46(19), 10834-10843,
 453 doi:10.1029/2019gl082873.
- 454 Lange, B. A., C. Katlein, G. Castellani, M. Fernández-Méndez, M. Nicolaus, I. Peeken, and H.
 455 Flores (2017b), Characterizing Spatial Variability of Ice Algal Chlorophyll a and Net Primary
 456 Production between Sea Ice Habitats Using Horizontal Profiling Platforms, *Frontiers in Marine
 457 Science*, 4(349), doi:10.3389/fmars.2017.00349.
- 458 Leppäranta, M., and R. Hakala (1992), The structure and strength of first-year ice ridges in the
 459 Baltic Sea, *Cold Reg. Sci. Tech.*, 20(3), 295-311, doi:[https://doi.org/10.1016/0165-
 460 232X\(92\)90036-T](https://doi.org/10.1016/0165-232X(92)90036-T).
- 461 Light, B., T. C. Grenfell, and D. K. Perovich (2008), Transmission and absorption of solar
 462 radiation by Arctic sea ice during the melt season, *J. Geophys. Res.-Oceans*, 113(C3),
 463 doi:10.1029/2006jc003977.
- 464 Light, B., D. K. Perovich, M. A. Webster, C. Polashenski, and R. Dadic (2015), Optical
 465 properties of melting first-year Arctic sea ice, *Journal of Geophysical Research: Oceans*,
 466 120(11), 7657-7675, doi:10.1002/2015JC011163.
- 467 Maslanik, J. A., C. Fowler, J. Stroeve, S. Drobot, J. Zwally, D. Yi, and W. Emery (2007), A
 468 younger, thinner Arctic ice cover: Increased potential for rapid, extensive sea-ice loss, *Geophys.
 469 Res. Lett.*, 34(24), L24501, doi:10.1029/2007gl032043.
- 470 Maslanik, J. A., J. Stroeve, C. Fowler, and W. Emery (2011), Distribution and trends in Arctic
 471 sea ice age through spring 2011, *Geophys. Res. Lett.*, 38, doi:10.1029/2011gl047735.
- 472 Massicotte, P., I. Peeken, C. Katlein, H. Flores, Y. Huot, G. Castellani, S. Arndt, B. A. Lange, J.
 473 É. Tremblay, and M. Babin (2019), Sensitivity of phytoplankton primary production estimates to
 474 available irradiance under heterogeneous sea ice conditions, *Journal of Geophysical Research:
 475 Oceans*, 124(8), 5436-5450.
- 476 Matthes, L. C., J. K. Ehn, S. L.-Girard, N. M. Pogorzelec, M. Babin, and C. J. Mundy (2019),
 477 Average cosine coefficient and spectral distribution of the light field under sea ice: Implications
 478 for primary production., *Elem Sci Anth*, 7(1), doi:<http://doi.org/10.1525/elementa.363>.
- 479 Meier, W. N., et al. (2014), Arctic sea ice in transformation: A review of recent observed
 480 changes and impacts on biology and human activity, *Rev Geophys*, 52(3), 185-217, doi:Doi
 481 10.1002/2013rg000431.
- 482 Melling, H., D. R. Topham, and D. Riedel (1993), Topography of the upper and lower surfaces
 483 of 10 hectares of deformed sea ice, *Cold Reg. Sci. Tech.*, 21(4), 349-369,
 484 doi:[https://doi.org/10.1016/0165-232X\(93\)90012-W](https://doi.org/10.1016/0165-232X(93)90012-W).

- 485 Melnikov, I. A. (1997), *The Arctic sea ice ecosystem*, edited, Cambridge Univ Press.
- 486 Melnikov, I. A., and L. L. Bondarchuk (1987), To the ecology of the mass aggregations of
487 colonial diatom algae under the Arctic drifting sea ice, *Okeanologiya*, 27(2), 317-321.
- 488 Mobley, C. D. (1994), *Light and water: radiative transfer in natural waters*, Academic Press.
- 489 Mobley, C. D., G. F. Cota, T. C. Grenfell, R. A. Maffione, W. S. Pegau, and D. K. Perovich
490 (1998), Modeling light propagation in sea ice, *IEEE Transactions on Geoscience and Remote
491 Sensing* 36(5), 1743-1749, doi:10.1109/36.718642.
- 492 Nicolaus, M., C. Katlein, J. Maslanik, and S. Hendricks (2012), Changes in Arctic sea ice result
493 in increasing light transmittance and absorption, *Geophys. Res. Lett.*, 39, L24501,
494 doi:10.1029/2012gl053738.
- 495 Nuber, A., L. Rabenstein, J. A. Lehmann-Horn, M. Hertrich, S. Hendricks, A. Mahoney, and H.
496 Eicken (2017), Water content estimates of a first-year sea-ice pressure ridge keel from surface-
497 nuclear magnetic resonance tomography, *Ann. Glaciol.*, 54(64), 33-43,
498 doi:10.3189/2013AoG64A205.
- 499 Parmeter, R. R., and M. D. Coon (1972), Model of pressure ridge formation in sea ice, *Journal
500 of Geophysical Research (1896-1977)*, 77(33), 6565-6575,
501 doi:<https://doi.org/10.1029/JC077i033p06565>.
- 502 Pavlov, A. K., T. Taskjelle, H. M. Kauko, B. Hamre, S. R. Hudson, P. Assmy, P. Duarte, M.
503 Fernández-Méndez, C. J. Mundy, and M. A. Granskog (2017), Altered inherent optical
504 properties and estimates of the underwater light field during an Arctic under-ice bloom of
505 *Phaeocystis pouchetii*, *Journal of Geophysical Research: Oceans*, 122(6), 4939-4961,
506 doi:<https://doi.org/10.1002/2016JC012471>.
- 507 Perovich, D. K. (1990), Theoretical estimates of light reflection and transmission by spatially
508 complex and temporally varying sea ice covers, *J. Geophys. Res.-Oceans*, 95(C6), 9557-9567,
509 doi:10.1029/JC095iC06p09557.
- 510 Pilfold, N. W., A. E. Derocher, I. Stirling, and E. Richardson (2014), Polar bear predatory
511 behaviour reveals seascape distribution of ringed seal lairs, *Population Ecology*, 56(1), 129-138,
512 doi:10.1007/s10144-013-0396-z.
- 513 Rabenstein, L., A. Nuber, J. A. Lehmann-Horn, M. Hertrich, S. Hendricks, A. R. Mahoney, and
514 H. Eicken (2013), Porosity of a sea-ice pressure ridge keel estimated on the basis of surface
515 nuclear magnetic resonance measurements.
- 516 Rampal, P., J. Weiss, and D. Marsan (2009), Positive trend in the mean speed and deformation
517 rate of Arctic sea ice, 1979–2007, *Journal of Geophysical Research: Oceans*, 114(C5), C05013,
518 doi:10.1029/2008JC005066.

- 519 Richter-Menge, J. A., and G. F. N. Cox (1985), Structure, Salinity and Density of Multi-Year
 520 Sea Ice Pressure Ridges, *Journal of Energy Resources Technology*, 107(4), 493-497,
 521 doi:10.1115/1.3231224.
- 522 Siegel, V., B. Bergström, J. O. Strömberg, and P. H. Schalk (1990), Distribution, size
 523 frequencies and maturity stages of krill, *Euphausia superba*, in relation to sea-ice in the Northern
 524 Weddell Sea, *Polar Biol.*, 10(7), 549-557, doi:10.1007/BF00233705.
- 525 Smith, T. G., M. O. Hammill, and G. Taugbøl (1991), A Review of the Developmental,
 526 Behavioural and Physiological Adaptations of the Ringed Seal, *Phoca hispida*, to Life in the
 527 Arctic Winter, *Arctic*, 44(2), 124-131.
- 528 Strub-Klein, L., and D. Sudom (2012), A comprehensive analysis of the morphology of first-year
 529 sea ice ridges, *Cold Reg. Sci. Tech.*, 82, 94-109,
 530 doi:<https://doi.org/10.1016/j.coldregions.2012.05.014>.
- 531 Sturm, M., J. Holmgren, and D. K. Perovich (2002), Winter snow cover on the sea ice of the
 532 Arctic Ocean at the Surface Heat Budget of the Arctic Ocean (SHEBA): Temporal evolution and
 533 spatial variability, *Journal of Geophysical Research: Oceans*, 107(C10), SHE 23-21-SHE 23-17,
 534 doi:<https://doi.org/10.1029/2000JC000400>.
- 535 Taskjelle, T., M. A. Granskog, A. K. Pavlov, S. R. Hudson, and B. Hamre (2017), Effects of an
 536 Arctic under-ice bloom on solar radiant heating of the water column, *Journal of Geophysical
 537 Research: Oceans*, 122(1), 126-138, doi:<https://doi.org/10.1002/2016JC012187>.
- 538 Timco, G. W., and R. P. Burden (1997), An analysis of the shapes of sea ice ridges, *Cold Reg.
 539 Sci. Tech.*, 25(1), 65-77, doi:[https://doi.org/10.1016/S0165-232X\(96\)00017-1](https://doi.org/10.1016/S0165-232X(96)00017-1).
- 540 Wadhams, P., and N. Toberg (2012), Changing characteristics of arctic pressure ridges, *Polar
 541 Science*, 6(1), 71-77, doi:<https://doi.org/10.1016/j.polar.2012.03.002>.
- 542 Warren, S. G., and R. E. Brandt (2008), Optical constants of ice from the ultraviolet to the
 543 microwave: A revised compilation, *Journal of Geophysical Research: Atmospheres*, 113(D14),
 544 doi:<https://doi.org/10.1029/2007JD009744>.
- 545 Williams, G. D., et al. (2013), Beyond Point Measurements: Sea Ice Floes Characterized in 3-D,
 546 *Eos, Transactions American Geophysical Union*, 94(7), 69-70, doi:10.1002/2013EO070002.
- 547 Williams, G. D., T. Maksym, J. Wilkinson, C. Kunz, C. Murphy, P. Kimball, and H. Singh
 548 (2015), Thick and deformed Antarctic sea ice mapped with autonomous underwater vehicles,
 549 *Nature Geosci*, 8(1), 61-67, doi:10.1038/ngeo2299.
- 550